Near-threshold electron-impact excitation of the vacuum-ultraviolet resonance transitions in Ne, Ar, Kr, and Xe

V. Zeman* and K. Bartschat

Department of Physics and Astronomy, Drake University, Des Moines, Iowa 50311

C. Norén[†] and J. W. McConkey

Department of Physics, University of Windsor, Windsor, Ontario, Canada N9B 3P4

Results of semirelativistic R-matrix calculations for electron-impact excitation of the $(np^6)\,^1S_0 \rightarrow np^5[n+1]s$ ($J=1$) transitions in the noble gases Ne ($n=2$), Ar ($n=3$), Kr ($n=4$), and Xe ($n=5$) are compared with experimental values for light polarizations and angle-integrated magnetic sublevel cross sections. The calculations focus on the near-threshold regime, where negative-ion resonances have a significant effect on the results. In light of the complexity of the structures, the agreement between theory and experiment is very encouraging. Nevertheless, further improvements in the theoretical treatment of both the target structure and the collision dynamics seem necessary. [S1050-2947(98)09708-X]

PACS number(s): 34.80.Dp

I. INTRODUCTION

Since the early days of collision physics, electron-impact excitation of atoms has played a central role in both basic research and numerous applications. One of the many observables that yields additional information to the angle-integrated total cross section is the standard polarization fraction of light emitted in a direction perpendicular to the incident beam [1]. Measurements of this polarization, which is related to the alignment, i.e., the nonisotropic occupation of magnetic sublevels in the collision process, not only allow for a detailed study of resonance phenomena (see, for example, the review by Heddle and Gallagher [2]), but their importance has also been recognized in many other fields [3].

Polarization fractions after excitation of noble gas targets have been investigated for a long time, with most recent contributions by groups at Lincoln [4], Münster [5], and Perth [6,7]. In most cases, however, the work concentrated on transitions in the visible wavelength regime where standard analyzers for linear and circular light can be used.

In a series of recent papers [8–10], to be referred to as I, II, and III below, we presented results of polarization studies of the vacuum-ultraviolet (vuv) resonance radiation emitted by the inert gases He (I), Ne (II), and Ar, Kr, Xe (III) after electron-impact excitation. Theoretical results for comparison with experiment were available only for the helium target; in fact, excellent agreement between the measurements and the predictions of a relatively simple 11-state nonrelativistic R-matrix (close-coupling) calculation was obtained below the $n=3$ thresholds (for details, see I). For higher impact energies, a detailed comparison becomes very complicated, due to the effects of cascades on the population of the radiating levels.

The theoretical situation was much less satisfactory, however, for the other noble gases Ne, Ar, Kr, and Xe that were investigated experimentally in II and III. In light of the strengths of the R-matrix method, particularly for the prediction of low-energy impact excitation in the resonance region, it seemed worthwhile to use this method for the heavier noble gases as well. The promise of this approach was further enhanced by the recent success of such calculations in modeling electron-impact excitation of Ne [11] and Kr [12]. The latter work also revealed additional insight into general patterns of atomic alignment.

In the present work we attempt to shed more light on the complicated, near-threshold resonance structure by investigating the light polarization, angle-integrated magnetic sublevel cross sections, and even structures due to individual partial wave contributions that can (only) be isolated in a calculation. Additional motivation for both the experimental and theoretical work has been given before [8–12], together with comprehensive lists of earlier reviews and recent work for polarization studies in the vuv, visible, and infrared wavelength region, and thus will not be repeated here. Full details of the experiment and attempts to classify the structures due to negative-ion resonances by using an analytic model [13] have been presented earlier [8–10] and so only a brief summary will be presented in Sec. II. In Sec. III we present the main features of the numerical model, followed by comparisons between theory and experiment in Sec. IV.

II. EXPERIMENTAL METHOD

A hemispherical analyzer was used to energy select and focus an electron beam through the target rare gas beam into a Faraday cup. Beam currents were in the range 4–20 nA with corresponding energy spreads of 80–160 meV. Radiation from the interaction region, emitted orthogonal to the electron beam, traversed a single-reflection polarization analyzer and was detected using a channel electron multiplier.

*Present address: Mathematics Department, University of Nottingham, Nottingham NG7 2RD, UK.

†Present address: MS183-601, Jet Propulsion Laboratory, Pasadena, CA 91190.

The orientation of the analyzer was set using a stepper motor under computer control. Data were normally collected at four orthogonal positions of the analyzer corresponding to detection of light polarized parallel and perpendicular to the electron beam axis [8]. Data from the detector were routed into the memories of a multichannel analyzer. The electron beam energy was scanned automatically so that the variation of the polarization as a function of energy could be obtained directly. Studies of the variation of the polarization with target gas pressure were carried out to ensure freedom from depolarizing effects such as imprisonment of resonance radiation. The base pressure prior to introduction of gas into the system was 0.2 μtorr. Background effects due, for example, to small contributions to the measured signals from the background gas in the system were accounted for as discussed in I.

Full details of the error analysis are also contained in I. The total error includes contributions from statistical uncertainties, from uncertainties in the background subtraction technique, and from uncertainties in the determination of the polarization efficiency of the analyzer. Systematic errors, such as those caused by possible mechanical misalignment of the analyzer system, were minimized by averaging data from different analyzer positions as discussed in I.

III. NUMERICAL METHOD

The calculations reported here were performed along the lines described by Zeman and Bartschat [11] for electron-impact excitation of neon. Therefore only the most important aspects will be summarized below.

A. The structure calculations

The N-electron target states Φ_i were represented as multiconfiguration expansions

$$\Phi_i(\mathbf{r}_1, \ldots, \mathbf{r}_N) = \sum_k c_{ik} \phi_k(\mathbf{r}_1, \ldots, \mathbf{r}_N). \qquad (3.1)$$

The expansion coefficients and the approximate target energies E_i^N were obtained by diagonalizing the target Hamiltonian H^N according to

$$\langle \Phi_i | H^N | \Phi_j \rangle = E_i^N \delta_{ij}. \qquad (3.2)$$

The configurations ϕ_k were constructed from a bound orbital basis consisting of self-consistent-field (SCF) orbitals. The radial components of these orbitals, $P_{nl}(r)$, were obtained using the CIV3 atomic structure package of Hibbert [14] with the nonrelativistic Hamiltonian H^N used in the optimization procedure. After the orbitals were obtained, the approximate Breit-Pauli Hamiltonian

$$H_{BP}^N = H^N + H_{mass}^N + H_D^N + H_{SO}^N, \qquad (3.3)$$

consisting of the nonrelativistic Hamiltonian and the one-electron relativistic mass correction, Darwin, and spin-orbit terms, was used in the description of the target states.

The input for starting the optimization procedure consisted of the Hartree-Fock orbitals for the respective ground states, as given in the tables of Clementi and Roetti [15]. Further valence orbitals were then constructed for the $np^5[n+1]s$ and $np^5[n+1]p$ states, with simultaneous reoptimization of the outermost p orbital of the ground state configuration. The latter ensured that this orbital was also a reasonable approximation for the excited states of interest. In addition, a d and the next higher s valence orbital were constructed to account for the most important channel coupling effects for all the states of interest. In the case of argon, we also constructed a $5\bar{p}$ pseudo-orbital to account for the differences of the $4p$ orbital that would be obtained if it were optimized separately on the various excited states with dominant configuration $3p^54p$. The effect of this orbital on the results obtained for the states with configuration $3p^54s$ will be discussed below.

In the next section we will present results obtained in 31-state close-coupling approximations, including all states (number given in parentheses) that could be constructed from the following configurations:

Ne:$2p^6$ (1); $2p^53s$(4); $2p^53p$(10); $2p^53d$(12); $2p^54s$(4)

Ar:$3p^6$ (1); $3p^54s$(4); $3p^54p$(10); $3p^53d$(12); $3p^55s$(4)

Kr:$4p^6$ (1); $4p^55s$(4); $4p^55p$(10); $4p^54d$(12); $4p^56s$(4)

Xe:$5p^6$ (1); $5p^56s$(4); $5p^56p$(10); $5p^55d$(12); $5p^57s$(4) .

As in the case of neon [11], the calculated energy level splittings of the states considered here compared very well with experimentally determined values [16] for all four targets, although some problems became apparent for Kr and particularly Xe, mostly due to the close spacing and the overlap of states with configurations ($4p^55p$, $4p^54d$) and ($5p^56p$, $5p^55d$), respectively. To correct as much as possible for the missing details in the structure calculations, we modified the R-matrix code of Berrington, Eissner, and Norrington [17] in such a way that not only the energy splittings between the various states could be reproduced in agreement with experiment, but the way in which this was achieved could be controlled in detail, most importantly by ensuring minimal adjustments in the diagonal terms of the Hamil-

tonian matrix for the channels coupled to the target states of interest. For such complex systems as those under consideration here, having this control is essential, due to the wealth of resonances associated with the various target thresholds.

B. The collision calculations

The R-matrix method is based upon the partitioning of configuration space into two regions whose boundaries intersect at a specified radial distance $r = a$. In the internal region, $r \leq a$, electron exchange and correlation between the scattered electron and the N-electron target are considered important and the $(N+1)$-electron system is treated as a closed system. In the external region, $r > a$, exchange between the scattered electron and the target is neglected.

In the internal region, the $(N+1)$-electron problem is treated similarly to a bound state and Eq. (3.2) is replaced by

$$(\psi_k | H_{BP}^{N+1} | \psi_k') = E_k^{N+1} \delta_{kk'}, \tag{3.4}$$

where the ψ_k are $(N+1)$-electron basis states and the parentheses indicate the finite range of integration from $r = 0$ to $r = a$. The boundary radius a was chosen in such a way that all bound orbitals (physical or pseudo) had fallen off in magnitude sufficiently to warrant the neglect of exchange.

The ψ_k basis states in the R-matrix method are independent of the energy of the $(N+1)$-electron system, and are expanded in the form

$$\psi_k(\mathbf{r}_1, \ldots, \mathbf{r}_N, \mathbf{r}) = \mathcal{A} \sum_{ij} a_{ijk} \Phi_i(\mathbf{r}_1, \ldots, \mathbf{r}_N, \hat{\mathbf{r}}) \frac{1}{r} u_j(r)$$

$$+ \sum_j b_{jk} \phi_j(\mathbf{r}_1, \ldots, \mathbf{r}_{N+1}). \tag{3.5}$$

Here the Φ_i are channel functions formed from all target states included in the expansion, the $u_j(r)$ are continuum orbitals, and the ϕ_j are $(N+1)$-electron bound configurations. The antisymmetrization operator $\mathcal{A}$ accounts for electron exchange between the continuum electron and the atomic electrons.

Since our calculations included relativistic effects explicitly, the atomic angular momentum needed to be coupled with that of the continuum electron to yield a total electronic angular momentum $\mathbf{J}_{tot}$ of the $(N+1)$-electron system. The magnitude of this quantum number, its z component, and the parity π_{tot} are conserved during the scattering process. Compared to a nonrelativistic model, this coupling scheme greatly increases the number of scattering channels and, therefore, the number of elements in the Hamiltonian for each partial wave symmetry $[J_{tot}, \pi_{tot}]$. The computational time required to diagonalize the Hamiltonian, i.e., to solve Eq. (3.4), is thus increased considerably. However, since this diagonalization is independent of the collision energy, it only needs to be performed once for each symmetry. This is a tremendous advantage of the R-matrix formalism. We have used partial waves up to $J_{tot} = 9/2$, with 25 continuum orbitals for each orbital angular momentum, to ensure converged results for energies up to about 5 eV above the highest $np^5[n+1]s$ state. In the 31-state calculations, up to 121 channels were coupled for each symmetry, causing the dimension of the Hamiltonian matrix to exceed 3000. In the
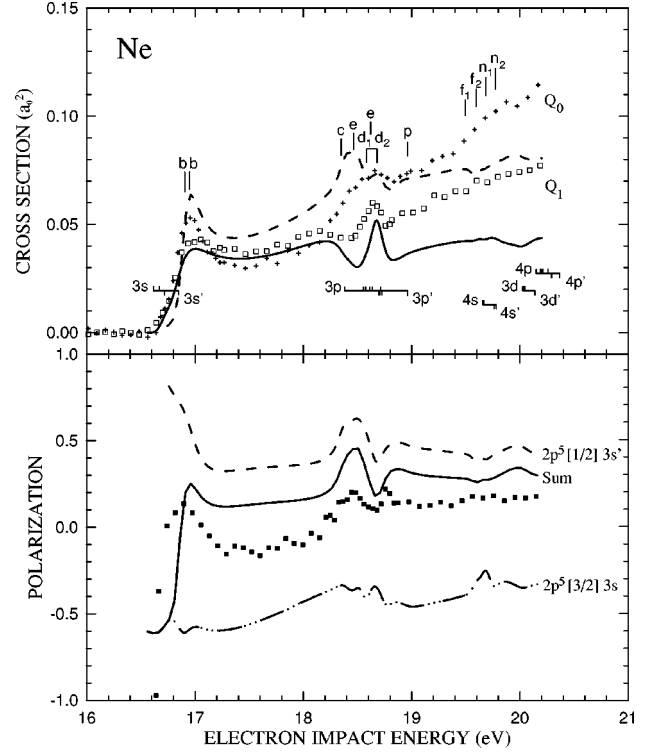

FIG. 1. Magnetic sublevel cross sections Q_0 and Q_1 (top, in units of a_0^2) and linear light polarization for electron-impact excitation of the $2p^5 3s$ and $2p^5 3s'$ ($J=1$) states in neon. The experimental data correspond to the weighted sum of contributions from both levels, but the light polarizations predicted for the individual states are also given. The thresholds of higher excited $2p^5 n\ell$ states and the resonance classification of Buckman and Clark [21] are also indicated.

41-state model for e-Ar scattering, the size of the calculation went up to 157 coupled channels and matrix sizes of nearly 4000.

Finally, the calculation for the external region was performed using the flexible asymptotic R-matrix (FARM) package by Burke and Noble [18]. For each collision energy, this yields the reactance ($\mathbf{K}$), scattering ($\mathbf{S}$), and transition ($\mathbf{T}$) matrices. Using standard procedures, these, in turn, can be used to obtain any observable of interest. For the present case of interest, see, for example, the book of Blum [19] and the paper by Bartschat *et al.* [20].

IV. RESULTS AND DISCUSSION

The lower parts of Figs. 1–4 show results for the polarization fraction P of the light emitted in the vuv transitions $2p^5[3/2]3s \rightarrow 2p^6$ and $2p^5[1/2]3s' \rightarrow 2p^6$ in Ne (Fig. 1), $3p^5[3/2]4s \rightarrow 3p^6$ and $3p^5[1/2]4s' \rightarrow 3p^6$ in Ar (Fig. 2), $4p^5[3/2]5s \rightarrow 4p^6$ and $4p^5[1/2]5s' \rightarrow 4p^6$ in Kr (Fig. 3), and $5p^5[3/2]6s \rightarrow 5p^6$ and $5p^5[1/2]6s' \rightarrow 5p^6$ in Xe (Fig. 4) as a function of the incident electron energy. Theoretical curves are given for the individual transitions as well as for their sum, obtained as a weighted average with the weights corresponding to the individual optical excitation cross sections for both lines. The experimental signal corresponds to this sum, plus any possible cascade contribution. All theoretical curves are from the 31-state Breit-Pauli R-matrix ap-
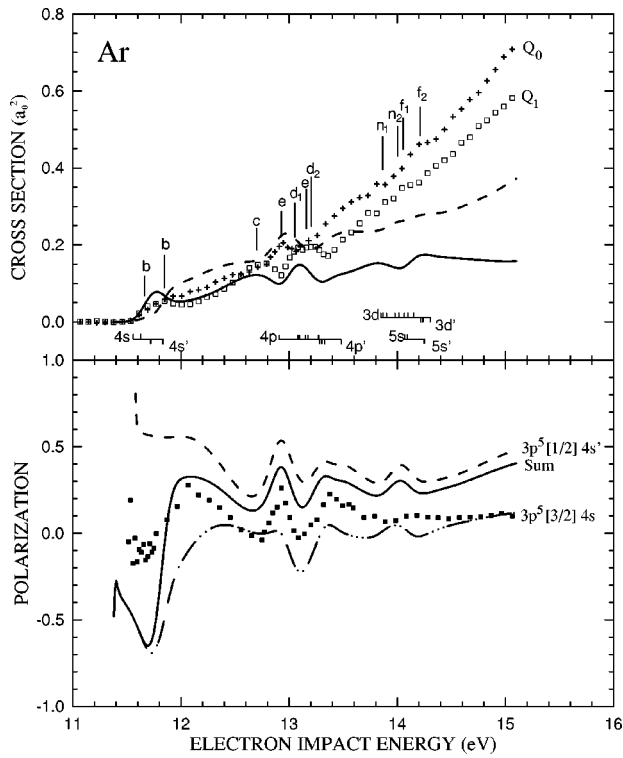
FIG. 2. Same as Fig. 1 for the $3p^5 4s$ and $3p^5 4s'$ ($J=1$) states in argon.

FIG. 4. Same as Fig. 1 for the $5p^5 6s$ and $5p^5 6s'$ ($J=1$) states in xenon.

proach described in the preceding section.

These light polarizations, after possible corrections for hyperfine-structure depolarization, finite experimental resolution, etc., are related to the magnetic sublevel cross sections Q_0 and Q_1, where the subscript denotes the z compo-
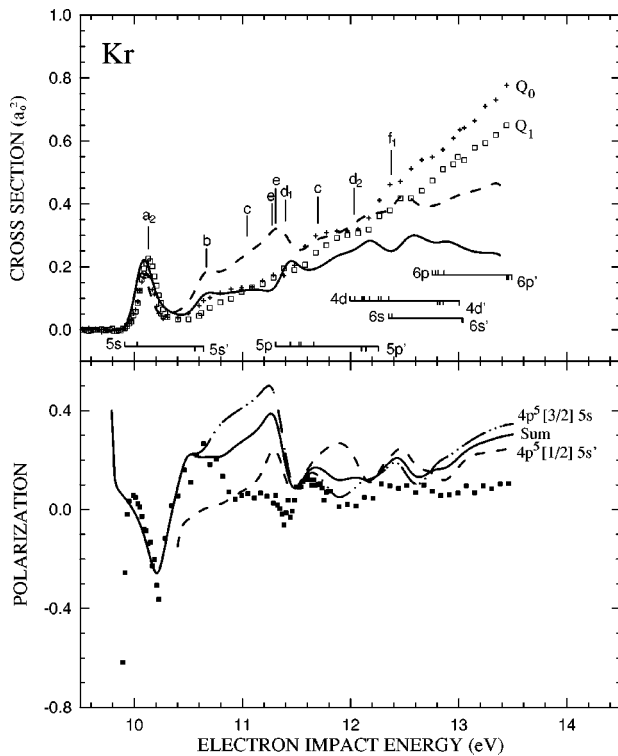

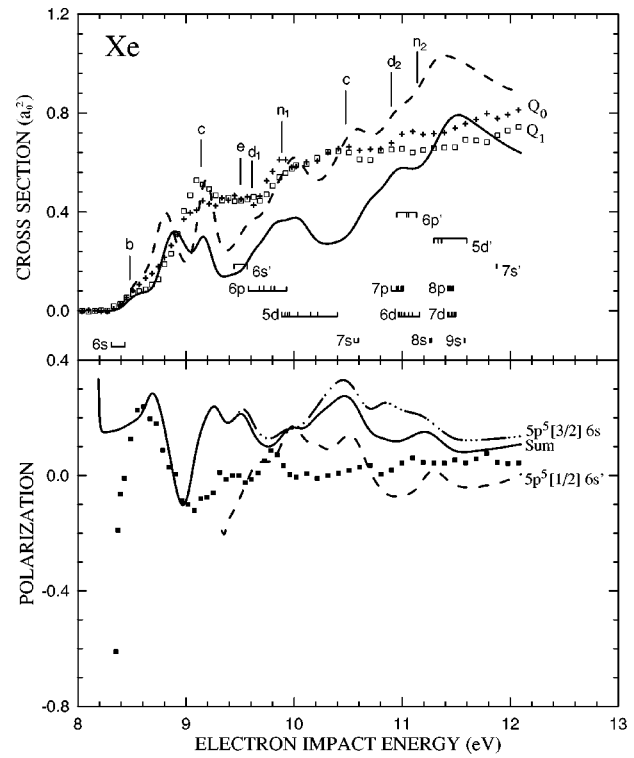FIG. 3. Same as Fig. 1 for the $4p^5 5s$ and $4p^5 5s'$ ($J=1$) states in krypton.

nent M_J of the total electronic angular momentum J ($=1$ for the excited states of interest in this work). In fact, the ratio of these sublevel cross sections, and therefore their relative size, can be extracted from the polarization measurement. [For details, see, for example, Eq. (3) of III.]

The upper parts of Figs. 1–4 show these magnetic sublevel cross sections, with the experimental data being normalized to give the best visual fit to the absolute theoretical results in the near-threshold region of the lowest resonance. The reasons for normalizing in this way are the following: (i) the agreement between theory and experiment in the shape of the curves is quite satisfactory in this region; (ii) especially in Kr and Xe, the thresholds of the two $J=1$ excited states are far enough apart so that only a signal from the lower state is measured right above threshold; (iii) cascades from excitation of the higher states (the thresholds are indicated in the figures) do not affect the results in this region. Also, the theoretical results have been convoluted with the energy width of the electron beam used in the experiment (80 meV for Ne and 160 meV for Ar, Kr, and Xe, respectively).

In light of the complexity of the structures, also indicated by the various resonance structures identified and classified by Buckman and collaborators (for an overview, see the review by Buckman and Clark [21]), the agreement between experiment and theory is quite encouraging. The remaining deviations between the measured data and the theoretical predictions, however, demonstrate the sensitivity of the polarization measurement as a detailed test of the theoretical model. This can be seen particularly in regions where one of the magnetic sublevel cross sections is overestimated while the other one is underestimated by theory; in such a case, the prediction of the total cross section would be much better than that of the individual contributions. We also note that
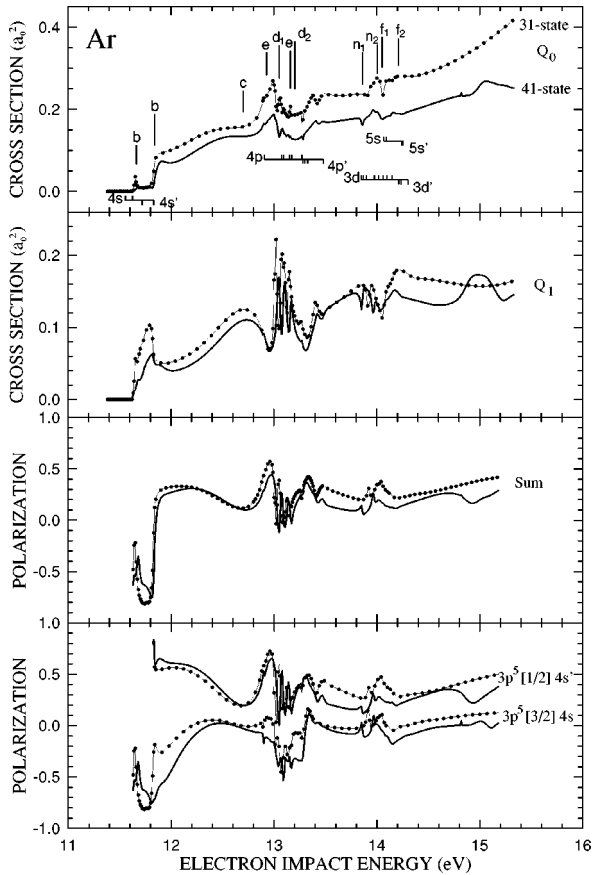
FIG. 5. Magnetic sublevel cross sections Q_0 and Q_1 (in units of a_0^2), averaged linear light polarization, and individual linear light polarizations for electron-impact excitation of the $3p^5 4s$ and $3p^5 4s'$ ($J=1$) states in argon, as obtained in 31-state and 41-state Breit-Pauli R-matrix calculations.

FIG. 6. Partial wave contributions to the cross section (in units of a_0^2) for electron-impact excitation of the $3p^5[3/2]4s$ ($J=1$) state in argon, as obtained in the 41-state Breit-Pauli R-matrix calculation.

cascade contributions to the observed signal begin as soon as the $np^5[n+1]p$ states can be excited. In general, these are expected to result in a net depolarization of the radiation, an effect that is clearly seen in all four experimental data sets. An *ab initio*, quantitative, theoretical treatment of these effects is nontrivial and will not be attempted here.

In our previous work on electron-impact excitation of neon [11], we showed how the representation of the $3p$ orbital in the states with configuration $2p^5 3p$ was very crucial for some of the results. In order to investigate such effects for the present work, we also performed a 41-state calculation for e-Ar scattering by including the ten states with configuration $3p^5 5\bar{p}$ in the close-coupling expansion as well. The $5\bar{p}$ orbital was constructed to minimize the sum of the theoretical energies of the $3p^5 4p$ states. The results obtained in the 31-state and 41-state calculations are shown in Fig. 5 for the magnetic sublevel cross sections (top), the measured polarizations (center), and the polarizations for the individual transitions (bottom). It is interesting to see that the result for the light polarization as a *relative* parameter is less sensitive to the details of the theoretical model than the *absolute* cross sections.

As the last item of this paper, we now discuss the possibility of analyzing the resonance structure in great detail by investigating contributions to the cross sections and the light polarization from individual partial waves. This will be illus-
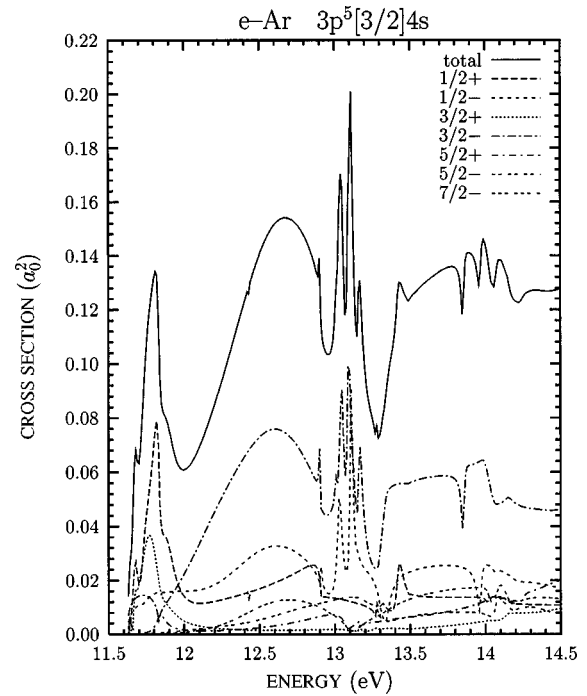
trated with the argon case as an example, mostly for excitation of the $3p^5[3/2]4s$ state.

We start by presenting in Fig. 6 the most important contributions to this cross section from partial waves with total $[J_{\text{tot}}, \pi_{\text{tot}}]$ symmetry, followed by even more details in Figs. 7 and 8, where we show the contributions from the $1/2+$ and $3/2-$ symmetries, split up even further into parts originating from various decay channels in the $j\ell K$ coupling scheme for the $(N+1)$-electron collision problem, where ℓ now denotes the orbital angular momentum of the continuum electron. While Fig. 6 looks very complex, we see that the biggest contribution to the "b" resonance around 11.7 eV incident energy comes, indeed, from the $1/2+$ channel with the scattered electron exiting via a p wave. This, together with similar results for excitation of the $3p^5[1/2]4s'$ state (not shown), clearly supports the assignment $3p^5(^2P^o_{3/2,1/2})4s4p(^3P^o)$ given by Buckman and Clark [21] to this set of resonances.

It is very interesting to note, however, that the theoretical polarization result (see Fig. 5) for the $3p^5[3/2]4s$ state is not even close to the zero value that one would obtain if only the $1/2+$ channel contributed to the signal (see Table V of [10]). Instead, the predicted polarization value for this state near 11.7 eV is close to its minimum of approximately -0.7. The other significant contributor to the cross section of the b resonances, namely, the $3/2+$ symmetry, can result in different values of the polarization even if it represents the only significant contribution (again we refer to Table V of [10]). To illustrate this, we therefore present in Fig. 9 the polarization obtained by taking into account individually the $3/2+$ and $3/2-$ contributions (the latter will be further discussed below). Since the $3/2+$ partial wave alone does not result in a significantly negative light polarization in this energy re-
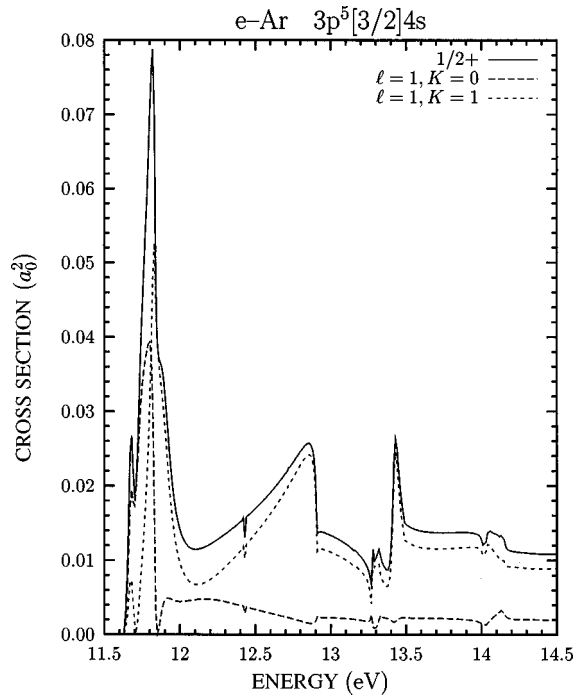
FIG. 7. Individual channel contributions to the cross section (in units of a_0^2) for electron-impact excitation of the $3p^5[3/2]4s$ ($J=1$) state in argon from the $1/2+$ symmetry, as obtained in the 41-state Breit-Pauli R-matrix calculation.

FIG. 9. Linear light polarizations predicted for electron-impact excitation of the $3p^5[3/2]4s$ ($J=1$) state in argon, if only the $3/2+$ or the $3/2-$ partial wave symmetries (individually) are taken into account, as obtained in the 41-state Breit-Pauli R-matrix calculation.

gion either, we are left with the conclusion that interference effects between different partial waves are most likely the source for this somewhat surprising result. In light of these findings, it would be most interesting to check the theory in
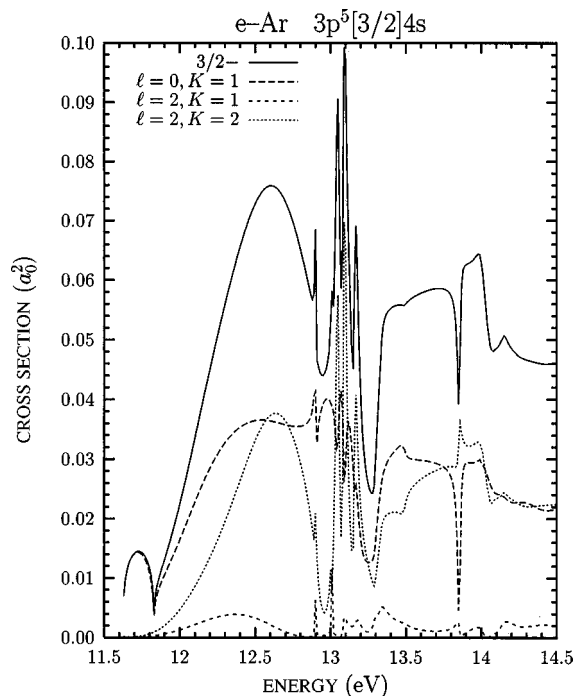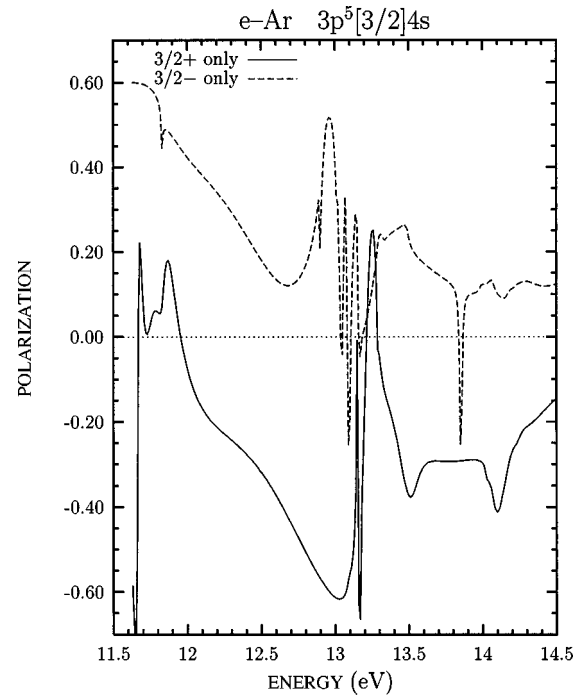

FIG. 8. Individual channel contributions to the cross section (in units of a_0^2) for electron-impact excitation of the $3p^5[3/2]4s$ ($J=1$) state in argon from the $3/2-$ symmetry, as obtained in the 41-state Breit-Pauli R-matrix calculation.

even more detail by comparing with an experimental result for the light polarization after excitation of the $3p^5[3/2]4s$ state alone.

Another interesting result of the present work concerns the energy region of the ''c'' resonance feature around 12.6 eV incident energy. As seen from Fig. 9, the dominant contribution comes from the $3/2-$ channel which, itself, is dominated by scattered electrons with orbital angular momentum $\ell=2$. Using parity conservation, these findings support assignments such as $3p^5(^2P^o_{3/2,1/2})4p^2(^1D)$ or $3p^5(^2P^o_{3/2,1/2})4s3d(^1D)$. In fact, this was already suggested by Ohja, Burke, and Taylor [22], for the ''c'' resonance, while Buckman and Clark [21] tentatively assigned the configuration $3p^5(^2P^o_{3/2,1/2})4s4p(^1P^o)$. Although examination of Fig. 9 indicates that interference effects between different partial waves are again too strong for the experiment alone to decide the configuration of the resonance, we believe that the good agreement between the measured and the predicted light polarizations in this energy region provides some additional credibility to the present theoretical results. This is a nice example of the necessary close interaction between experiment and theory in order for both to advance.

V. CONCLUSIONS

In summary, we have presented results from highly sophisticated numerical calculations for electron-impact excitation of the vuv emitting states in Ne, Ar, Kr, and Xe, and have compared the results with recent experimental data. The

satisfactory agreement obtained between theory and experiment gives us confidence in the interpretation of the results, particularly with respect to the resonance classification in e-Ar collisions. The remaining differences between theory and experiment clearly call for further improvement of the theoretical model, both with respect to the structure description of the target and the treatment of the collision itself. Especially for Ne and Ar, where the use of nonrelativistic one-electron orbitals seems justifiable, a semirelativistic version of the R matrix with pseudo-states approach [23] is certainly very promising. Work in this direction is currently in progress.

[1] H.W.B. Skinner and E.T.S. Appleyard, Proc. R. Soc. London, Ser. A **117**, 224 (1927).

[2] D.W.O. Heddle and J.W. Gallagher, Rev. Mod. Phys. **61**, 221 (1989); D.W.O. Heddle, Contemp. Phys. **17**, 443 (1976), and references therein .

[3] S.A. Kazantsev and J.-C. Hénoux, *Polarization Spectroscopy of Ionized Gases* (Kluwer Academic, Boston, 1995).

[4] J.E. Furst, W.M.K.P. Wijayaratna, D.H. Madison, and T.J. Gay, Phys. Rev. A **47**, 3775 (1993).

[5] M. Uhrig, G.F. Hanne, and J. Kessler, J. Phys. B **27**, 4009 (1994).

[6] D.H. Yu, P.A. Hayes, J.F. Williams, and J.E. Furst, J. Phys. B **30**, 1799 (1997).

[7] D.H. Yu, P.A. Hayes, J.E. Furst, and J.F. Williams, Phys. Rev. Lett. **78**, 2724 (1997).

[8] C. Norén, J.W. McConkey, P. Hammond, and K. Bartschat, Phys. Rev. A **53**, 1559 (1996).

[9] C. Norén and J.W. McConkey, Phys. Rev. A **53**, 1559 (1996).

[10] C. Norén, W.L. Karras, J.W. McConkey, and P. Hammond, Phys. Rev. A **54**, 510 (1996).

[11] V. Zeman and K. Bartschat, J. Phys. B **30**, 4609 (1997).

[12] V. Zeman, K. Bartschat, T.J. Gay, and K.W. Trantham, Phys. Rev. Lett. **79**, 1825 (1997).

[13] A. Wolcke, K. Bartschat, K. Blum, H. Borgmann, G.F. Hanne, and J. Kessler, J. Phys. B **16**, 639 (1983).

[14] A. Hibbert, Comput. Phys. Commun. **9**, 141 (1975).

[15] E. Clementi and C. Roetti, At. Data Nucl. Data Tables **14**, 177 (1974).

[16] C.E. Moore, *Atomic Energy Levels*, Natl. Bur. Stand. Ref. Data Ser., Natl. Bur. Stand. (U.S.) Circ. No. 35 (U.S. GPO, Washington, DC, 1971).

[17] K.A. Berrington, W.B. Eissner, and P.H. Norrington, Comput. Phys. Commun. **92**, 290 (1995).

[18] V.M. Burke and C.J. Noble, Comput. Phys. Commun. **85**, 471 (1995).

[19] K. Blum, *Density Matrix Theory and Applications*, 2nd ed. (Plenum, New York, 1996).

[20] K. Bartschat, N.S. Scott, K. Blum, and P.G. Burke, J. Phys. B **17**, 269 (1984).

[21] S.J. Buckman and C.W. Clark, Rev. Mod. Phys. **66**, 539 (1994).

[22] P.C. Ohja, P.G. Burke, and K.T. Taylor, J. Phys. B **15**, L507 (1982).

[23] K. Bartschat, E.T. Hudson, M.P. Scott, P.G. Burke, and V.M. Burke, J. Phys. B **29**, 115 (1996); Phys. Rev. A **54**, R998 (1996).